XANES Study of Cu 2+ Binding Sites in Aquatic Humic Substances

ARTICLE *in* ENVIRONMENTAL SCIENCE AND TECHNOLOGY · JUNE 2000

Impact Factor: 5.33 · DOI: 10.1021/es990561u

3 AUTHORS, INCLUDING:

Gregory V Korshin
University of Washington Seattle
126 PUBLICATIONS **2,247** CITATIONS

Environ. Sci. Technol. **2000**, *34,* 2138−2142

XANES Study of Cu^{2+}-Binding Sites in Aquatic Humic Substances

ANATOLY I. FRENKEL,[†,‡] GREGORY V. KORSHIN,*[,§] AND ALEXEI L. ANKUDINOV[||]

Materials Research Laboratory, University of Illinois at Urbana−Champaign, Urbana, Illinois 61801, Department of Civil and Environmental Engineering, University of Washington, Box 352700, Seattle, Washington 98195-2700, and Physics Department, University of Washington, Box 351560, Seattle, Washington 98195-1560

The structure and composition of the inner shell of copper (II) complexes with aquatic humic substances (HS) were studied by X-ray absorption near-edge structure (XANES) spectroscopy. The interpretation of the XANES data was based on FEFF8 code real-space multiple-scattering calculations for the prototype $[Cu(H_2O)_6]^{2+}$ complex. These calculations reproduced the tetragonal distortion of the CuO_6 octahedron representing the inner shell. They also demonstrated the polarization nature of this effect's manifestations ("splitting" of the derivative) in XANES. The extension of this interpretation to the Cu−HS system confirmed suppression of the tetragonal distortion of the inner shell in these species established by independent EXAFS experiments. XANES measurements for Cu/C ratios varying from 0.0005 to 0.03 demonstrated the nonuniform nature of copper binding sites. Experiments with Cu−ethylenediamine and Cu−glycine model systems and FEFF8 calculations indicated that for low copper concentrations (Cu/C < 0.005) nitrogen-containing functional groups dissimilar to those of amino acids are likely to be engaged in the complexation.

Introduction

ESR, IR, spectrophotometric, and potentiometric data relevant to the formation of Cu^{2+}−HS complexes indicate that the first complexation shell in these species may be described as a tetragonally distorted CuO_6 octahedron. The oxygens in the first complexation shell have been associated with carboxylic-, salicylic-, and phthalic-type ligands (*1*−*9*). Soil and sludge HS also contain nitrogen whose weight contribution may be as high as 10% (*4*−*6*), but in aquatic HS it is typically <1% (*10*). The relevant nitrogen-containing entities have been hypothesized to be amine, α-aminocarboxylic, or porphyrin functional groups associated with chlorophyll and proteins residues (*1*−*3, 8, 9*). The nitrogen belonging to these groups has been hypothesized to enter the inner complexation shell and form a $CuO_{6-x}N_x$ structure (*4, 5, 7*). Despite the evidence qualitatively attesting to the relevance of these hypotheses, the actual presence and number of N atoms in the octahedron, the identities of the functional groups, and the lengths/strength of the Cu−O and Cu−N bonds have been difficult to establish due to the polydisperse nature of HS, the lack of long-term order in solutions/solids containing HS, and problems with finding model compounds that could adequately reproduce the behavior of HS. Some of these difficulties may be circumvented through the use of X-ray absorption fine structure (XAFS) spectroscopy, notable for its ability to probe highly disordered systems with great structural and chemical sensitivity (*11*−*22*). Two modifications of XAFS [extended X-ray absorption fine-structure (EXAFS) and X-ray absorption near-edge structure (XANES)] measure the X-ray absorption coefficients in different energy regions relative to the absorption edge of the target atom and yield complementary information about the sample. For both techniques, the energy dependence of X-ray absorption coefficient is governed by Fermi's golden rule, which takes into account the final state of the photoelectron ejected from the target atom due to the absorption of X-ray quanta and the electronic densities of unoccupied states (DOS) (*23*). The EXAFS oscillations observed for energies >40 eV past the X-ray absorption edge are adequately described solely by the photoelectron scatterings from the neighboring atoms (*24, 25*). The range of a XANES spectrum is assigned to the energies between the first symmetry-allowed unoccupied state and the continuum states, that is ca. < 40 eV past the absorption edge. XANES contains information about the electronic structure, DOS, and bonding geometry around the absorbing atom (*26*). The interpretation of XANES is more complex than that of EXAFS and is based on both the multiple scattering expansion and the DOS. Full multiple scattering calculations are essential in the XANES data analysis (*27*), but until recently, the theoretical simulation and interpretation of XANES spectra for arbitrary systems, especially for those with hydrogen atoms, have been either unavailable or very difficult (*28, 29*). In this work, our goal is to further probe the local structure around the metal ion in the Cu−HS system through the state-of-the-art modeling of XANES spectra using FEFF8 computer code. We will also explore the manifestations of nonuniformity of metal binding sites in HS by carrying out XANES measurements of the Cu−HS system at varying Cu/C ratios.

Experimental Section

The hydrophobic acids fraction (HPOA) from Suwannee River natural organic matter and HS from Judy Reservoir (JRHS) were used in the experiments. The preparation and properties of these HS samples were described in Korshin et al. (*15*) and in more detail in Croué et al. (*30*). HPOA contained 0.7% nitrogen and 0.3% sulfur. Its elemental composition was very close to that previously reported for Suwannee River fulvic acid (*10*). The DOC concentration in all HS-containing solutions was 1000 mg/L. The desired amount of metal was added as $Cu(ClO_4)_2$. The Cu/C molar ratios were 0.0005, 0.00125, 0.0025, 0.005, 0.0125, and 0.03. The pH of solutions containing HS and copper was 4.0. Model systems included copper(II) aqua-complex $[Cu(H_2O)_6]^{2+}$ and copper complexes with ethylenediamine and glycine (denoted as EN and Gly, respectively). The metal and ligand concentrations in solutions containing copper and the model ligands were 0.01 and 0.1 M, respectively. The metal concentration in solutions containing only copper aqua-complex was 0.1 M. $[Cu(H_2O)_6]^{2+}$ and Cu−Gly solution were prepared at pH 4, and Cu−EN was prepared at pH 12.

The X-ray absorption measurements were carried out at the X11-A and X16-C beamlines of the National Synchrotron

* Corresponding author phone: (206)543-2394; fax: (206)685-9185; e-mail: korshin@u.washington.edu.

[†] Materials Research Laboratory.

[‡] Mailing address: Brookhaven National Laboratory, Building 510 E, Upton, New York 11973.

[§] Department of Civil and Environmental Engineering.

[||] Physics Department.

10.1021/es990561u CCC: $19.00
Published on Web 04/14/2000

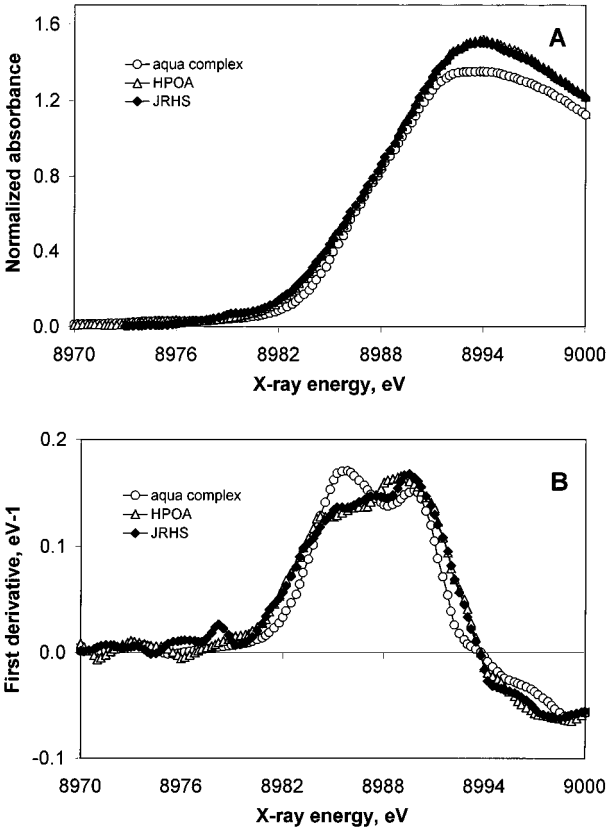

FIGURE 1. X-ray absorption spectra (A) and their derivatives (B) in the Cu K-edge XANES region for $[Cu(H_2O)_6]^{2+}$, Cu−JRHS, and Cu−HPOA. Cu/C = 0.03, pH 4.

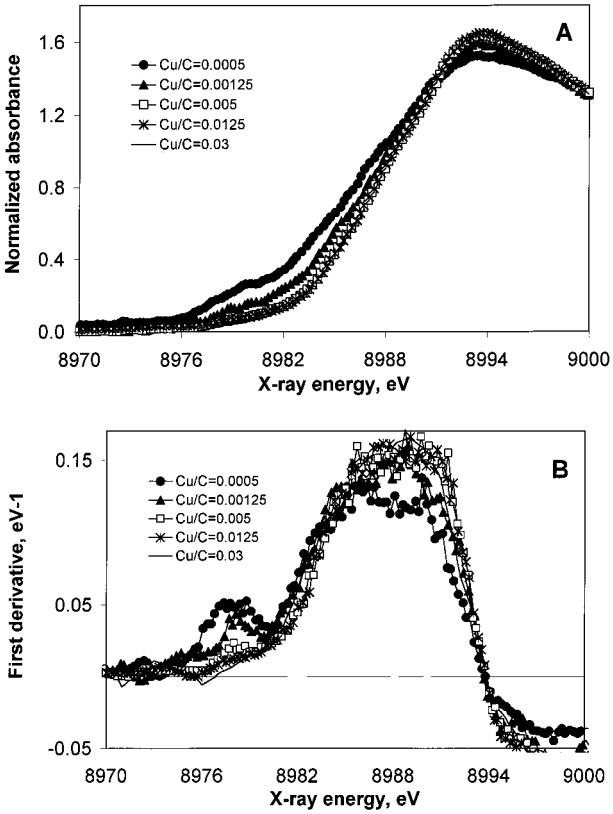

FIGURE 2. X-ray absorption spectra (A) and their derivatives (B) in the Cu K-edge XANES region for Cu−HPOA solutions at varying Cu/C ratios, pH 4.

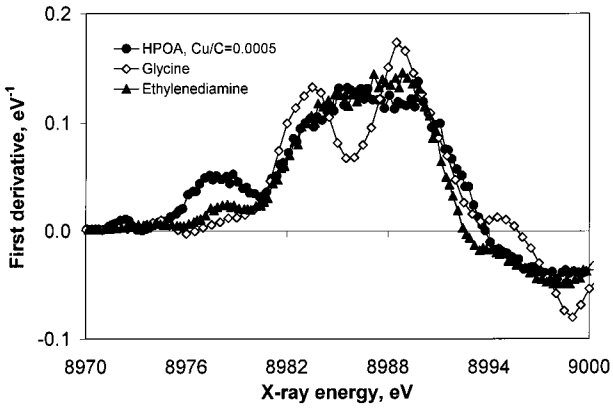

FIGURE 3. First derivatives of the X-ray absorption spectra in the Cu K-edge XANES region for Cu−HPOA solution (Cu/C = 0.0005) at pH 4, and reference Cu−ethylenediamine (pH 12) and Cu−glycine (pH 4) complexes.

Light Source at Brookhaven National Laboratory using experimental settings identical to those reported in ref *15*. The X-ray energy varied from 200 eV below to 400 eV above the absorption K edge of Cu (E_K = 8979 eV) using a Si(111) double-crystal monochromator. The data were obtained in the fluorescence mode. To compare the state of Cu^{2+} in HS-containing solutions with varying Cu/C ratios, the pre-edge and near-edge regions of the data (-30 eV < $E-E_K$ < 40 eV) were acquired with a 0.5-eV energy increment. The EXAFS data (the range 40 eV < $E-E_K$ < 400 eV) were also acquired with a 2-eV increment. To improve the signal-to-noise ratio, up to 20 measurements were averaged for the same sample. To correct for a small angular drift of the monochromator crystals between the scans, all data sets were aligned vs their absolute energy and interpolated to the same 0.25-eV increment grid before the averaging. Copper metal foil was always measured in the transmission mode simultaneously with all other samples and was used as the reference for the alignment of energies.

Experimental Data and Their Interpretation

In this paper, we will discuss only the XANES features corresponding to the 1s → 4p transitions located in the region 8979−8995 eV. The Cu K-edge region XANES spectra and their first derivatives for $[Cu(H_2O)_6]^{2+}$, Cu−HPOA, and Cu−JRHS solutions (Cu/C = 0.03) are shown in Figure 1, panels A and B, respectively. The $[Cu(H_2O)_6]^{2+}$ data were notably different from those for all other samples. The derivative XANES spectrum of $[Cu(H_2O)_6]^{2+}$ had two prominent maxima at 8985.8 and 8989.8 eV. The features of the derivative XANES spectra of Cu^{2+}−HS complexes were less prominent, while the data for Cu−HPOA and Cu−JRHS complexes were virtually similar. The width of the first derivative spectrum for $[Cu(H_2O)_6]^{2+}$ at its half-maximum was almost 2 eV narrower as compared to that in all other samples at pH 4.

The increase of the Cu/C ratios in the Cu−HS system was accompanied by a pronounced and consistent change of a pre-edge feature located between 8976 and 8980 eV (Figure 2, panels A and B). In the XANES derivative spectra normalized by the maximum of their intensity, this feature was most intense for the lowest Cu/C ratio (0.0005) and gradually lost its intensity with the increase of the copper concentration. At the Cu/C ratio of 0.03 used in our previous paper (*15*), it was undetectable. The derivative XANES spectra for Cu−HPOA for the lowest copper concentration (Cu/C = 0.0005) and for the model systems (Cu−EN and Cu−Gly) are compared in Figure 3. These data demonstrated that of all the reference systems, the shoulder in the X-ray absorption coefficient in the range of 8976−8980 eV was detected only for the Cu−EN complex.

Thus, the XANES spectra of copper(II) complexes were affected by the type of ligand and by the Cu/C ratio. However, their quantitative interpretation is complicated by the necessity to account for effects associated with the composition of the CuO_xN_{6-x} octahedron, distances between the Cu^{2+} ion and its nearest neighbors, their respective disorders, charge transfer from the first shell atoms to the central ion, and contributions from next nearest neighbors. Given these limitations, it is necessary to explore first the interpretation of the XANES spectra for simple models. In this paper, this is done through the analysis of the XANES spectra of the $[Cu(H_2O)_6]^{2+}$ prototype system based on FEFF8 modeling. The splitting of the derivative XANES spectrum for $[Cu(H_2O)_6]^{2+}$ has been attributed to the tetragonal distortion of the CuO_6 octahedron caused by the Jahn−Teller effect (*31, 32*). The shoulder on the main absorption edge jump below the maximum results from the superposition of the two polarized contributions of the CuO_6 octahedra whose ***z*** axis is oriented either parallel or perpendicular to the polarization of the electric field vector ***e*** (***e***||***z*** and ***e***||***x,*** respectively) (*31*). Since the CuO_6 octahedra are randomly oriented in solutions, the ***e***||***z*** and ***e***||***x*** contributions are averaged in proportion of 1:2. The spectrum for the ***e***||***z*** polarization exhibits a maximum at the energy lower than that for the ***e***||***x*** polarization. The energy separation between these two maxima has been qualitatively related to the difference between the equatorial and the axial Cu−O distances in the CuO_6 octahedron, but the empirical equation derived by Garcia et al. (*31*) significantly overestimated the observed distortion (*33*). Multiple scattering calculations carried out by Palladino et al. (*32*) confirmed the polarization nature of the splitting of the XANES spectrum for $[Cu(H_2O)_6]^{2+}$, while Benfatto et al. (*29*) improved the calculations by including hydrogen atoms of the water molecules.

The FEFF8 computer code (*28*) advances the modeling of XANES spectra by using self-consistent, full multiple scattering calculations of both the electronic structure and XANES. FEFF8 is the first XANES code to obtain self-consistency within the real space Green's function approach. The importance of self-consistency in XANES calculations was demonstrated earlier by, for example, Foulis et al. and Natoli et al. (*34, 35*). However, FEFF8 is the first XANES code to obtain the exact position of the Fermi level and to account for the charge transfer effects between the target atom and its neighbors. In the earlier codes (e.g., FEFF6 (*36*)), the Fermi level and charge transfers were used as fitting parameters, thus significantly reducing the prediction power of the XANES code. It is specifically undesirable in our case since our goal is to estimate the axial Cu−O length in $[Cu(H_2O)_6]^{2+}$ and thereby to evaluate the effects of the tetragonal distortion on the splitting of the maxima in the XANES derivatives.

The ab initio FEFF8 modeling of the XANES spectra for $[Cu(H_2O)_6]^{2+}$ was performed without any a priori presumptions regarding the charges on the oxygens in the CuO_6 octahedron. In accord with the literature data (*15−17, 33, 37−42*), the equatorial Cu−O distance was set at 1.97 Å. The only variable in these calculations was the axial Cu−O distance, which is more difficult to establish experimentally as compared with that for the equatorial bond due to the high disorder inherent for this bond. The derivative XANES spectra calculated for the axial Cu−O distance varying from 2.10 to 2.40 Å are shown in Figure 4. The best agreement between the experimental and the calculated XANES data were found for the axial distance between 2.20 and 2.30 Å. This agrees well with the independent results reported in refs *15, 33, 37−40,* and *42*.

In agreement with Benfatto et al. (*29*), the inclusion of hydrogen atoms in the model was found to notably improve the agreement between the theory and the experimental data since otherwise the predicted axial Cu−O distance in $[Cu(H_2O)_6]^{2+}$ was unrealistically large (ca 2.50 Å). However, there is a difficulty in regards to the inclusions of hydrogen atoms in the muffin-tin potential approximation. This difficulty exists because the O−H bond is much shorter than the Cu−O distance, and for the oxygen it is difficult to determine a good muffin-tin radius. In FEFF8, this was circumvented by assuming phase transferability for the hydrogen atoms. It was assumed that the partial wave phase shifts do not significantly depend on the O−H distance. Although this premise has limitations, its use is well justified for the hydrogen atoms because they are weak scatterers even in XANES. On the basis of this approach, the procedure for the self-consistent calculations was as follows: The O−H distance was increased to ca. 1.5 Å, and the partial wave phase shifts were calculated for this configuration. For the final calculations of XANES or density of states, the original geometry was restored, but the phase shifts and Fermi level were taken from the artificially shifted geometry. This sequence of calculations had been tested for the Pu^{3+} and Pu^{6+} hydrates, and it worked very well (*43*).

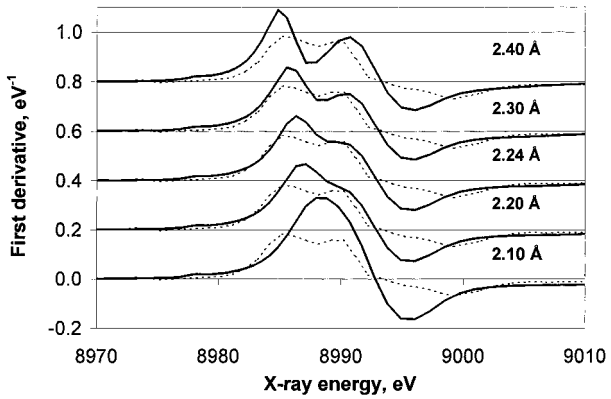

FIGURE 4. First derivatives (solid lines) of the simulated Cu K-edge XANES in the $[Cu(H_2O)_6]^{2+}$ complex for varying axial Cu−O_{ax} distances. The equatorial Cu−O_{eq} distance is fixed at 1.97 Å. Experimental data are shown with dashed lines.

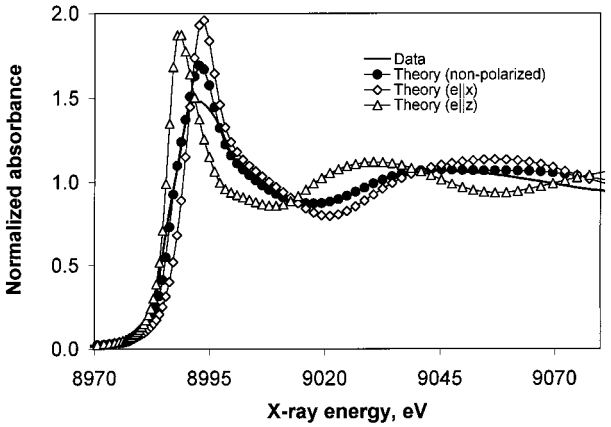

FIGURE 5. Comparison of the experimental and simulated Cu K-edge XANES spectra for $[Cu(H_2O)_6]^{2+}$. Equatorial and axial Cu−O distances used in the FEFF8 simulations were 1.97 and 2.24 Å, respectively. The theoretical XANES spectra calculated for two different polarizations are also shown.

Figure 5 additionally demonstrates the polarization nature of the shoulder of the XANES spectra located approximately in the middle of the edge jump. The XANES signal calculated for the ***e***||***z*** polarization is shifted toward lower energies as compared to that for the ***e***||***x*** polarization. This result also agrees well with the literature (*31−33*). The summation of the ***e***||***z*** and ***e***||***x*** signals (weighted with a 1:2 ratio) follows the experimental data fairly closely in region up to ca. 80 eV

above the copper K edge. This additionally supports the validity of the simulation results obtained in the vicinity of the X-ray absorption edge.

The FEFF8 results for the axial bond length set at 2.24 Å [this value was obtained from the EXAFS data analysis in our previous publication (*15*)] are also shown in Figure 4. The higher intensity of the calculated spectrum in the vicinity of the lower-energy derivative (energy range of 8984−8989 eV) may be an evidence of a strong disorder in the axial Cu−O bond length observed experimentally by EXAFS. Indeed, FEFF8 simulations assume zero disorder (quantified by σ^2 in EXAFS measurements) for all the Cu−O bonds. This assumptions is valid as long as the disorder of the bond length is small, since the Debye−Waller factor term $\exp(-2k^2\sigma^2)$ affecting the magnitude of the X-ray absorption coefficient is very close to unity for small k, i.e., in XANES region. In our case, however, both the wavenumber (k = 1.8 Å^{-1}) and disorder ($\sigma^2 = 0.04$ Å^2) (*15*) for the axial bonds are large enough to explain the suppression of the $\boldsymbol{e}||\boldsymbol{z}$ contribution relative to the prediction by the FEFF8 theory, as seen in the experiment in the 1s → 4p transition region. The suppression of the XANES signal is much less pronounced for the $\boldsymbol{e}||\boldsymbol{x}$ polarization contribution to XANES (higher-energy peak in the derivative, Figure 9) associated with the equatorial Cu−O bonds since the corresponding σ^2 is much smaller (0.004 Å^2). Given the omission of the disorder effects in the model used, it appears that the agreement between the theory and the experiment might be even better than that shown in Figure 4.

The XANES modeling data for $Cu[H_2O]_6^{2+}$ can be used to interpret those of the Cu^{2+}−HS system. The splitting of the first derivatives of the Cu−HS system is less prominent than in the $[Cu(H_2O)_6]^{2+}$ data (Figure 1B). On the basis of the data of XANES modeling, this indicates a lesser degree of tetragonal distortion of the CuO_6 octahedron for the copper(II)−HS complexes. This agrees well with the data of our previous EXAFS study and that of several other independent sources (*15*−*17*). However, it needs to be recognized that the tetragonal distortion of the CuO_6 system in complexes other than $[Cu(H_2O)_6]^{2+}$ is not necessarily caused solely by the Jahn−Teller effect but also may be related to the presence of nonidentical ligands in the inner shell (*16, 17*), which may weaken or completely cancel the tetragonal distortion. Our XANES data indicate that, independent of the origin of the tetragonal distortion of the CuO_6, this distortion is certainly considerably smaller for Cu−HS systems than for $[Cu(H_2O)_6]^{2+}$.

Aside from confirming the data of independent EXAFS studies of the inner shell structure of Cu^{2+}−HS complexes (*15*), the XANES data clearly demonstrate the nonuniformity of copper-binding sites in HS. This issue was not addressed in the previous XAFS studies of metal−HS interactions. Figure 2, panels A and B, shows a specific XANES feature located in the range of 8975−8980 eV and observed at low Cu/C ratios. The origin of this feature is intriguing. Our FEFF8 simulations showed that, in this energy region, XANES features cannot be associated with the Cu−O bonds since these contribute to the X-ray absorption at higher energies (8980−8995 eV). The ESR data (*4, 5, 7*−*9*) indicate that at low Cu/C ratios, Cu^{2+} is likely to form complexes with nitrogen-containing functional groups, although the exact identification of these ligands has not been possible. To ascertain the origin of this feature, theoretical simulations were carried out in which 1, 2, or 4 equatorial water molecules in $[Cu(H_2O)]_6^{2+}$ were replaced by NH_3 groups, whose nitrogen atoms were placed at 1.8, 1.9, or 2.0 Å from the central Cu^{2+} ion. The FEFF8 code modeling of the XANES spectra for the $CuO_{6-x}N_x$ corresponding system showed that the appearance of the nitrogen atoms in the inner shell was accompanied by the development of a distinct pre-edge feature located in the range of energies lower than the main jump of the X-ray absorption coefficient (Figure 6). The location of this feature was analogous to that observed in the experiment for Cu/C ratios <0.005. The calculations also indicated that the Cu−N distance of 2.0 Å was more plausible as compared with the distances of 1.8 or 1.9 Å. However, these results have a qualitative meaning since the changes of the Cu−O distances in the inner shell that are likely to occur upon the introduction of the nitrogen atoms in the $CuO_{6-x}N_x$ octahedron were not accounted for but fixed at 1.92 and 2.13 Å for the equatorial and axial bonds in Cu^{2+}−HS complexes in accordance with our previous EXAFS results (*15*). Further theoretical ab initio XANES calculations of the composite oxygen- and nitrogen-containing inner shell will answer these questions in more detail. Nevertheless, on the basis of both comparison with the XANES spectra of the reference systems and theoretical calculations, we conclude that the features observed in the XANES spectra of the Cu^{2+}−HS system at low Cu/C ratios are likely to be a manifestation of complexation with nitrogen-containing functional groups.

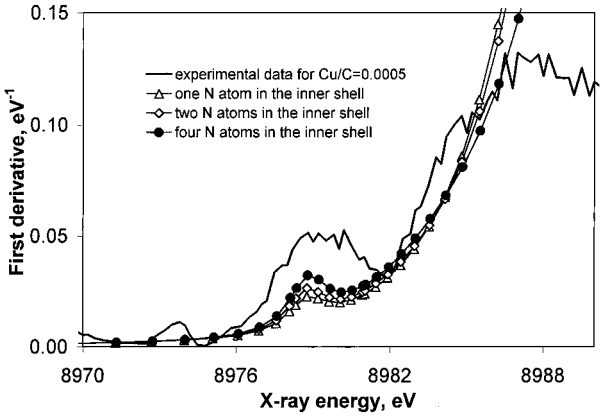

FIGURE 6. Influence of the nitrogen incorporation in the first complexation shell of Cu^{2+}. Results of FEFF8 simulation. Axial and equatorial Cu−O distances fixed at 1.92 and 2.13 Å, respectively. Cu−N distance 2.00 Å.

The pre-edge features associated with the nitrogen-containing groups were not observed for the complexes of copper with glycine and were recorded solely for ethylenediamine. Glycine was selected since it is one of the predominant amino acids found in HPOA and other aquatic HS (*10, 30, 44*). The fact that the copper(II)−glycine system is not representative for the copper−HS complexation at low Cu/C ratios may be interpreted in several ways. First, amino acids dissimilar to glycine may predominate in the formation of complexes at low metal dosages. Second, the structural properties of amino acids bound to the HS backbone may be different from those of free amino acids. Third, the nitrogen-containing complexation sites in aquatic HS may be fundamentally dissimilar to the amino carboxylic group. The latter point concurs with the literature data indicating that, in Suwannee River fulvic acid, only ca. 9% of the organic nitrogen could be associated with amino acids while the chemical status of the remaining nitrogen has not been ascertained (*10*).

Despite the clear need for further experimentation needed to elucidate the chemical nature of the nitrogen in HS, the results presented here support and significantly enhance the hypotheses that nitrogen-containing groups are likely to preferentially bind copper(II) at low Cu/C ratios. Their spectral manifestations (e.g., the pre-edge feature in XANES) gradually disappear with the increase of the copper concentration, in which case the complexation with much more abundant carboxyl groups becomes predominant. This was seen both in this work (Figure 2A,B) and in our previous

paper (*15*), which demonstrated that the structural parameters of the CuO_6 octahedron are similar (but not identical) to those of the complexes of Cu^{2+} with salicylic acid.

The agreement between XANES and EXAFS results demonstrates the possibility to employ XANES to probe the structure of the metal−HS complexes and to ascertain and quantify the nonuniformity of the metal-binding sites. The latest XANES experiments and simulations opens yet unexplored possibilities to obtain structural information for solutions with very low metal concentrations, for which the EXAFS signal is likely to be too weak to be reliably processed. In this work, the XANES measurements were carried out for solutions with Cu concentrations as low as 4.2×10^{-5} M, but it is recognized that in order to study the state of heavy metals in noncontaminated water samples, the threshold metal concentration needs to be lowered by orders of magnitude. This necessitates the use of the third-generation X-ray synchrotron sources. We have conducted preliminary experiments at the UNI−CAT 33-ID beamline (Advanced Photon Source, Argonne National Laboratory) whose beam intensity is ca. 2 orders of magnitude higher than that at BNL to obtain XANES spectra of a Cu−HS system with metal concentrations lower than those used in this work. The relevant data will be described elsewhere.

Acknowledgments

The authors express their appreciation to Profs. Mark Benjamin (University of Washington, Seattle, WA), Chi-Wang Li (Tamkang University, Taipei, Taiwan), Jean-Philippe Croué (University de Poitiers, Poitiers, France), and Dr. Jerry Leenheer (U.S. Geological Survey, Denver, CO) for characterization of the HS samples and participation in the discussion on their intrinsic chemistry. A.I.F. acknowledges support by DOE Grant DEFG02-96ER45439 through Materials Research Laboratory at the University of Illinois at Urbana−Champaign. G.V.K. acknowledges support from the American Water Works Research Foundation (Projects 159-94 and 2563-98) and the U.S. Environmental Protection Agency (Grant R826645).

Literature Cited

(1) McKnight, D. M.; Wershaw, R. L. In *Humic Substances in the Suwannee River, Georgia: Interactions, Properties, and Proposed Structures*; Open File Report 87-557; U.S. Geological Survey: Denver, 1989; p 59−79.
(2) Ephraim, J. H.; Marinsky, J. A. *Anal. Chim. Acta* **1990**, *232*, 171−185.
(3) Ephraim, J. H.; Marinsky, J. A. *Environ. Sci. Technol.* **1986**, *20*, 367−383.
(4) Boyd, S. A.; Sommers, L. E.; Nelson, D. W.; West, D. X. *Soil Sci. Soc. Am. J.* **1981**, *45*, 745−749.
(5) Boyd, S. A.; Sommers, L. E.; Nelson, D. W.; West, D. X. *Soil Sci. Soc. Am. J.* **1983**, *47*, 43−46.
(6) Boyd, S. A.; Sommers, L. E.; Nelson, D. W. *Soil Sci. Soc. Am. J.* **1981**, *45*, 1241−1242.
(7) Senesi, N. *Anal. Chim. Acta* **1990**, *232*, 51−75.
(8) Mangrich, A. S.; Lermen, A. W.; Santos, E. J.; Gomes, R. C.; Coelho, R. R. R.; Linhares, L. F.; Senesi, N. *Biol. Fertil. Soils* **1998**, *26*, 341−345.
(9) Bloom, P. R.; McBride, M. B. *Soil Sci. Soc. Am. J.* **1979**, *43*, 687−692.
(10) Thurman, E. M.; Malcolm, R. L. *Humic Substances in the Suwannee River, Georgia: Interactions, Properties, and Proposed Structures*; Open File Report 87-557; U.S. Geological Survey: Denver, 1989; pp 99−118.
(11) Xia, K.; Weesner, F.; Bleam, W. F.; Bloom, P. R.; Skyllberg, U. L.; Helmke, P. A. *Soil Sci. Soc. Am. J.* **1998**, *62*, 1240−1246.
(12) Denecke, M. A.; Reich, T.; Pompe, S.; Bubner, M.; Heise, K. H.; Nitsche, H.; Allen, P. G.; Bucher, J. J.; Edelstein, N. M.; Shuh, D. K.; Czerwinski, K. R. *Radiochim. Acta* **1998**, *82*, 103−108.
(13) Rose, J.; Vilge, A.; Olivie-Lauquet, G.; Masion, A.; Frechou, C.; Bottero, J. Y. *Colloids Surf. A* **1998**, *136*, 11−19.
(14) Davies, G.; Fataftah, A.; Cherkasskiy, A.; Ghabbour, E. A.; Radwan, A.; Jansen, S. A.; Kolla, S.; Paciolla, M. D.; Sein, L. T.; Buermann, W.; Balasubramanian, M.; Budnick, J.; Xing, B. S. *J. Chem. Soc., Dalton Trans.* **1997**, *21*, 4047−4060.
(15) Korshin, G. V.; Frenkel, A. I.; Stern, E. A. *Environ. Sci. Technol.* **1998**, *32*, 2699−2705.
(16) Xia, K.; Bleam, W.; Helmke, P. A. *Geochim. Cosmochim. Acta* **1997**, *61*, 2211−2221.
(17) Xia, K.; Bleam, W. F.; Helmke, P. A. *Geochim. Cosmochim. Acta* **1997**, *61*, 2223−2235.
(18) Vairavamurthy, M. A.; Maletic, D.; Wang, S. K.; Manowitz, B.; Eglinton, T.; Lyons, T. *Energy Fuels* **1997**, *11*, 546−553.
(19) Morra, M. J.; Fendorf, S. E.; Brown, P. D. *Geochim. Cosmochim. Acta* **1997**, *61*, 683−688.
(20) Vairavamurthy, M. A.; Manowitz, B.; Maletic, D.; Wolfe, H. *Org. Geochem.* **1997**, *26*, 577−585.
(21) Sarret, G.; Manceau, A.; Hazemann, J. L.; Gomez, A.; Mench, M. *J. Phys. IV Fr.* **1997**, *7*, C2-799−802.
(22) Manceau, A.; Boisset, M. C.; Sarret, G.; Hazemann, R. L.; Mench, M.; Cambier, P.; Prost, P. *Environ. Sci. Technol.* **1996**, *30*, 1540−1552.
(23) Stern, E. A.; Heald, S. M. In *Handbook on Synchrotron Radiation*; Koch, E. E., Ed.; North-Holland: Amsterdam, 1983.
(24) Sayers, D. A.; Stern, E. A.; Lytle, F. W. *Phys. Rev. Lett.* **1971**, *27*, 1204.
(25) Stern, E. A.; Sayers, D. A.; Lytle, F. W. *Phys. Rev. B* **1975**, *11*, 4836−4846.
(26) Stöhr, J. *NEXAFS Spectroscopy*; Springer-Verlag: Berlin, 1992
(27) Durham P. J.; Pendry J. B.; Hodges C. H. *Comput. Phys. Commun.* **1982**, *25*, 193−205.
(28) Ankudinov, A. L.; Ravel, B.; Rehr, J. J.; Condradson, S. D. *Phys. Rev. B* **1998**, *58*, 7565−7576.
(29) Benfatto, M.; Solera, J. A.; Chaboy, J.; Proietti, M. G.; Garcia, J. *Phys. Rev. B* **1997**, *56*, 2447−2452.
(30) Croué, J.-P.; Korshin, G. V.; Leenheer, J. A.; Benjamin, M. M. *Isolation, Fractionation and Characterization of Natural Organic Matter in Drinking Water*; AWWA Research Foundation and American Water Works Association: Denver (in press).
(31) Garcia, J.; Benfatto, M.; Natoli, C. R.; Bianconi, A.; Fontaine, A.; Tolentino, H. *Chem. Phys.* **1989**, *132*, 295−302.
(32) Palladino, L.; Della Longa, S.; Reale, A.; Belli, M.; Scafati, A.; Onori, G.; Santucci, A. *J. Chem. Phys.* **1993**, *98*, 2720−2726.
(33) Nomura, M.; Yamaguchi, T. *J. Phys. Chem.* **1988**, *92*, 6157−6160.
(34) Foulis, D. L.; Pettifer, R. F.; Sherwood, P. *Europhys. Lett.* **1995**, *29*, 647−653.
(35) Natoli, C. R.; Misemer, D. K.; Doniach, S.; Kutzler F. W. *Phys. Rev. A* **1980**, *22*, 1104−1115.
(36) Zabinsky, S. I.; Rehr, J. J.; Ankudinov, A.; Albers, R. C.; Eller, M. J. *Phys. Rev. B* **1995**, *52*, 2995−3009.
(37) Beagley, B.; Eriksson, A.; Lindgren, J.; Persson, I.; Pettersson, L. G. M.; Sandstrom, M.; Wahlgren, U.; White, E. W. *J. Phys.: Condens. Matter* **1989**, *1*, 2395−2408.
(38) D'Angelo, P.; Bottari, E.; Festa, M. R.; Nolting, H.-F.; Pavel, N. V. *J. Chem. Phys.* **1997**, *107*, 2807−2812.
(39) Musinu, A.; Paschina, G.; Piccaluga, G.; Magini, M. *Inorg. Chem.* **1983**, *22*, 1184−1187.
(40) Ozutsumi, K.; Miyata, Y.; Kawashima, T. *J. Inorg. Biochem.* **1991**, *44*, 97−108.
(41) Ozutsumi, K.; Kawashima, T. *Inorg. Chim. Acta* **1991**, *180*, 231−238.
(42) Tabata, M.; Ozutsumi, K. *Bull. Chem. Soc. Jpn.* **1994**, *67*, 1608−1614.
(43) Ankudinov, A. L.; Conradson, S. D.; Rehr, J. J. *Phys. Rev. B* **1998**, *57*, 7518−7525.
(44) Thurman, E. M. *Organic Geochemistry of Natural Waters*; Martin Nijhoff and W. Junk, Publishers: Dordrecht, The Netherlands, 1985.

Received for review May 17, 1999. Revised manuscript received November 19, 1999. Accepted March 3, 2000.

ES990561U